Preference of Proteomonas Sulcata Anion Channelrhodopsin for Nitrate Revealed Using a pH Electrode Method

Chihiro Kikuchi
Division of Soft Matter, Graduate School of Life Science, Hokkaido University
Hina Kurane
Division of Soft Matter, Graduate School of Life Science, Hokkaido University
Takuma Watanabe
Division of Macromolecular Functions, Department of Biological Science, School of Science, Hokkaido University
Makoto Demura
Faculty of Advanced Life Science, Hokkaido University
Takashi Kikukawa
Faculty of Advanced Life Science, Hokkaido University
Takashi Tsukamoto (t-tak@sci.hokudai.ac.jp)
Faculty of Advanced Life Science, Hokkaido University

Research Article

Keywords: light-gated anion channelrhodopsins (ACRs), ion pump rhodopsins, living organisms

Posted Date: February 1st, 2021

DOI: https://doi.org/10.21203/rs.3.rs-153619/v1

Version of Record: A version of this preprint was published at Scientific Reports on April 12th, 2021. See the published version at https://doi.org/10.1038/s41598-021-86812-z.

Preference of *Proteomonas sulcata* anion channelrhodopsin for nitrate revealed using a pH electrode method

Chihiro Kikuchi[1], Hina Kurane[1], Takuma Watanabe[2], Makoto Demura[3,4], Takashi Kikukawa[3,4] & Takashi Tsukamoto[3,4,*]

[1] Division of Soft Matter, Graduate School of Life Science, Hokkaido University, Sapporo 060-0810, Japan.
[2] Division of Macromolecular Functions, Department of Biological Science, School of Science, Hokkaido University, Sapporo 060-0810, Japan.
[3] Faculty of Advanced Life Science, Hokkaido University, Sapporo 060-0810, Japan.
[4] Global Station for Soft Matter, Global Institution for Collaborative Research and Education, Hokkaido University, Sapporo 001-0021, Japan.

[*]Corresponding author: Takashi Tsukamoto
Phone & Fax: +81 11 706 4475
Email: t-tak@sci.hokudai.ac.jp

Abstract

Ion channel proteins are physiologically important molecules in living organisms. Their molecular functions have been investigated using electrophysiological methods, which enable quantitative, precise and advanced measurements and thus require complex instruments and experienced operators. For simpler and easier measurements, we measured the anion transport activity of light-gated anion channelrhodopsins (ACRs) using a pH electrode method, which has already been established for ion pump rhodopsins. Using that method, we successfully measured the anion transport activity and its dependence on the wavelength of light, i.e. its action spectra, and on the anion species, i.e. its selectivity or preference, of several ACRs expressed in yeast cells. In addition, we identified the strong anion transport activity and the preference for NO_3^- of an ACR from a marine cryptophyte algae *Proteomonas sulcata,* named *Psu*ACR_353. Such a preference was discovered for the first time in microbial pump- or channel-type rhodopsins. Nitrate is one of the most stable forms of nitrogen and is used as a nitrogen source by most organisms including plants. Therefore, *Psu*ACR_353 may play a role in NO_3^- transport and might take part in NO_3^--related cellular functions in nature. Measurements of a mutant protein revealed that a Thr residue in the 3rd transmembrane helix, which corresponds to Cys102 in *Gt*ACR1, contributed to the preference for NO_3^-. These findings will be helpful to understand the mechanisms of anion transport, selectivity and preference of *Psu*ACR_353.

Introduction

In living cells, there are several kinds of proteins that transport a variety of ions and small molecules across cell membranes. The membrane transport of those substrates is directly or indirectly connected to a variety of life phenomena, such as the maintenance of cell homeostasis, cell signaling, the generation of action potential in neurons, and so on. Therefore, membrane transport proteins are physiologically important and their molecular properties, including their structures and functions, have been intensively investigated by many research groups. In this study, we focused on one type of ion transporter, ion channels.

Ion channels passively transport ions according to the electrochemical potential gradients of ions across cell membranes. No external energy is needed for that type of transport, however some factors, such as membrane potential change, binding of ligands as well as physical or mechanical stimuli, are necessary to open and close those channels. In 2002, the first light-gated ion channel-type microbial rhodopsin for cations (cation channelrhodopsin, abbreviated as CCR) was reported, which originated from a green algae *Chlamydomonas reinhardtii* and was named channelrhodopsin-1 (abbreviated as ChR1) [1]. As the name suggested, channelrhodopsins belong to a family of microbial rhodopsins, each composed of a seven transmembrane α-helical protein opsin and a chromophore all-*trans*-retinal [2]. A year later, another CCR that originated from the same algae, named channelrhodopsin-2 (abbreviated as ChR2), was reported [3]. ChR1 selectively transports H^+, whereas ChR2 transports not only H^+ but also other monovalent cations, such as Li^+, Na^+ and K^+ [1,3]. In 2015, natural light-gated anion channelrhodopsins (abbreviated as ACRs) that originated from a cryptophyte algae *Guillardia theta*, named *Gt*ACR1 and *Gt*ACR2, were reported [4]. Both of those ACRs are capable of transporting monovalent anions, such as F^-, Cl^-, Br^-, I^- and NO_3^- [4]. Since then, many more CCRs and ACRs have been identified, characterized and engineered [5-25]. Especially for ACRs, they are novel proteins that have just been discovered and therefore their molecular characteristics and their biological roles remain to be clarified.

The molecular functions of ion channels have been investigated using several experimental techniques. Especially, electrophysiological methods, such as the patch-clamp method, are highly quantitative and accurately characterize ion channel functions. In cases of not only ACRs but also CCRs, a series of electrophysiological analyses, such as current-voltage relationship and ion selectivity or preference, have been precisely

performed. In addition, the introduction of a short-pulsed laser as an actinic light source into the electrophysiological measurement system enables the measurement of transient current changes during a single sequential photochemical reaction of microbial rhodopsins, called the photocycle [2,15,16,19,26,27]. This technique is beneficial for identifying which photo-intermediates facilitate ion conducting and non-conducting states in the photocycle. Therefore, electrophysiological analysis is powerful and necessary to deeply understand the ion channel mechanisms of ACRs and CCRs. However, in exchange for such accuracy, complex instrumental setups and experienced operators are required. This is a bottleneck not only for non-experts in electrophysiology but also for scientists who want to measure ion transport activity more simply and easily.

We conceived the idea to measure the anion transport activity of ACRs using the pH electrode method, which had already been established for ion pump-type microbial rhodopsins expressed as recombinant proteins in *Escherichia coli* cells. Simple instrumental setups and usability of the pH electrode method are a great advantage although the method is less quantitative compared to the electrophysiological method. In addition, the pH electrode method is expected to easily measure the dependence of the activities of ACRs on the wavelength of excitation light, i.e. action spectra, and on the anion species, i.e. selectivity or preference, even if precise measurements for reversal potentials, current density, kinetics, and so on, are impossible to perform. However, *E. coli* cells cannot be used as host cells to express a variety of recombinant ACRs except for *Gt*ACR2 [28-30]. In most cases so far, insect, mammalian and yeast cells have been used as host cells for the expression of recombinant ACRs. Among them, yeast cells are as easy to culture as *E. coli* cells and to exchange buffers for the measurement of anion transport activity. Therefore, the pH electrode method is expected to be applicable for ACRs expressed in yeast cells to measure anion transport activity and anion dependence in a relatively simple way.

In this research study, we first developed and demonstrated the feasibility of the pH electrode method to measure the anion transport activity of ACRs expressed in yeast cells. We used *Gt*ACR1, which is a well-studied ACR at present, to test the usefulness of the system. The action spectrum and anion dependence of the activity of *Gt*ACR1 measured using the pH electrode method were almost the same as previously measured using the electrophysiological method [4]. To apply this method to other ACRs, we measured the anion transport activities of 7 ACRs that were successfully expressed in

yeast cells. As a result, we found that an ACR that originated from a marine cryptophyte algae *Proteomonas sulcata*, previously named as *Psu*ACR_353 [18], showed the strongest activity among the ACRs that we tested and preferably transported nitrate (NO_3^-) to other monovalent anions, such as Cl^- and Br^-. NO_3^- is one of the most stable forms of nitrogen on earth and is used as a nitrogen source by most organisms including plants [31]. Therefore, the light-gated *Psu*ACR_353 may play a role in NO_3^- transport and might possibly take part in nitrate sensing and signaling, and furthermore, the nitrogen assimilation by *P. sulcata* in nature. Measurement of a mutant protein revealed that the Thr108 residue in the 3rd transmembrane helix, which corresponds to Cys102 in *Gt*ACR1, contributed to the NO_3^- preference in *Psu*ACR_353. These findings will be helpful to understand the mechanisms of anion transport, selectivity and preference of *Psu*ACR_353.

Results

Concept of the pH electrode method. Fig. 1 illustrates the concept of the pH electrode method for measuring the anion transport activity of ACRs expressed in yeast cells. The fundamental concept was almost the same as that for the system using *E. coli* cells. The yeast cell suspension was poured into the glass vial container and the pH electrode was placed into it. The cell suspension was stirring during the measurement to keep the suspension homogeneous. Continuous LED light (10 mW/cm^2 on average) was illuminated for 2 min from the side of the vial container. To reduce undesirable artifacts, we were careful not to let the light directly hit the light-sensitive part of the pH electrode.

Yeast cells have a cell wall outside and a cell membrane inside and ACRs are localized in the cell membrane. Once the light activated ACRs, anions were passively transported into the cells due to the electrochemical potential gradient of anions being higher outside the cells (300 mM) than inside (nearly 0 mM). This anion influx resulted in making the membrane potential more negative. To compensate for that, protons (H^+) in the bulk solution penetrate into the cells by passing through the cell wall and cell membrane. As a result, we can indirectly observe anion transport using the pH electrode as a pH change of the suspension. In this study, we observed pH increases that reflect the anion transport into yeast cells.

Demonstration of the pH electrode method to measure the activity of *Gt*ACR1. To ensure that the system works, we used *Gt*ACR1 as a test sample. First, we successfully expressed *Gt*ACR1 in yeast *P. pastoris* cells according to previous studies [27,32]. We then measured the Cl^- transport activity of *Gt*ACR1 using the pH electrode method, and as shown in Fig. 2a, the activity of *Gt*ACR1 was successfully measured. The signal for the pH increase was clearly larger than that of control cells, in which no ACR gene was integrated. In most cases for anion and sodium-ion pump rhodopsins, the measurements were carried out in the presence of a proton-selective ionophore, carbonyl cyanide m-chlorophenyl hydrazone (abbreviated as CCCP), which facilitates the proton influx into cells. As a result, the signal of the pH change becomes larger than that in the absence of CCCP. Conversely, this tendency is evidence for rhodopsins being capable of transporting anions or sodium ions but not protons. However, in the case of *Gt*ACR1, the signal intensity of the pH change was decreased in the presence of CCCP (Fig. 2a) although protons are not transport substrates of *Gt*ACR1 [4]. We concluded that the decrease in signal intensity in the presence of CCCP was caused by the denaturation of *Gt*ACR1, which was indicated by the color change of the cell suspension from pink to yellow (Fig. 2b). Therefore, all subsequent measurements were carried out in the absence of CCCP.

We then measured the dependence of the excitation light wavelength on the Cl^- transport activity, i.e. the action spectrum (Fig. 2c). Stronger signals were obtained when the sample was illuminated using 505 nm and 530 nm light than by using 590 nm light. The amplitudes of the initial slope obtained from each condition were averaged and were statistically compared (Fig. 2d). As a result, the activities at 505 nm and 530 nm were not significantly different but were stronger than that at 590 nm. This result correlated well with the absorption spectrum of purified *Gt*ACR1 (Fig. 2e) and with the action spectrum previously measured using the electrophysiological method [4]. Therefore, the pH electrode method can be used to investigate the action spectra of ACRs.

The anion-dependent transport activity of *Gt*ACR1 was also measured using 530 nm LED light for activation. Six monovalent anions (F^-, Cl^-, Br^-, I^-, NO_3^- and aspartate (abbreviated as Asp^-)) and one divalent anion (SO_4^{2-}) at a concentration of 300 mM were tested (Figs. 2f and 2g). As a result, significant transport activities were obtained for the anions except for F^- and Asp^- compared to the negative control cells. As suggested by a previous electrophysiological study [4], the anion selectivity of *Gt*ACR1

was not so restricted. Therefore, the pH electrode method in this study closely reproduced such a dependence. Therefore, we concluded that the pH electrode method can potentially be applied to measure anion transport activity, the action spectrum and the anion dependence of ACRs expressed in yeast cells.

Application of the pH electrode method to other ACRs. The pH electrode method was then used to test other ACRs. At present, several ACR genes have been identified by transcriptome analysis. Among them, we tested 8 ACRs (3 from *Proteomonas sulcata* and 5 from *Geminigera cryophila*; see Table 1) for functional expression in yeast cells. Five of the 8 ACRs tested in this study belong to the Cys-type (see below) as does *Gt*ACR1, 2 belong to the Thr-type as does RapACR reported recently [18], and 1 belongs to the Val-type as does *Gt*161302 reported previously [4]. Note that *G. cryophila* has 5 ACRs that belong to all three types.

ACRs can be roughly classified into three types, the Cys-type, the Thr-type and the Val-type (Fig. 3a). One of the factors contributing to that classification is the amino acid conserved at position 102 in *Gt*ACR1. It has been reported that two amino acid residues contribute to the channel gating of *Gt*ACR1 [26,27]. One is Glu68 located in the 2nd transmembrane helix that controls slow-opening/fast-closing gates (Table 1 and Supplementary Fig. S1). Another is Cys102 located in the 3rd transmembrane helix that regulates fast-opening/slow-closing gates. The Glu residue is completely conserved in all ACRs we tested, whereas the Cys residue is substituted with Thr or Val (Table 1, Fig. 3a, and Supplementary Fig. S1). For the case of the recently reported RapACR, the Thr residue corresponding to Cys102 in *Gt*ACR1 was also shown to contribute to the channel gating kinetics [18]. However, the effect of such diversity in the amino acid conservation on anion transport activity, anion selectivity or preference is not well understood. No anion transport activity was reported for *Gt*161302, which has a Val residue corresponding to Cys102 in *Gt*ACR1 [4].

As shown in Fig. 3b, 7 of the 8 ACRs, except *Gc*ACR_439, were pigmented in the presence of all-*trans*-retinal, indicating their successful expression in yeast cells. We then measured the Cl^- transport activities for these ACRs using the pH electrode method. For activation, 505 nm LED light was used for ZipACR, *Gc*ACR_145 and *Gc*ACR_457, while 530 nm LED light was used for *Psu*ACR1, *Psu*ACR_353, *Gc*ACR_197 and *Gc*ACR_201, by taking into account the colors of the cells and the action spectral maxima

reported previously [15-18]. The intensity of light was kept at an average of 10 mW/cm^2. As a result, the signals of pH change were obtained in most ACRs but the intensities were very weak (Fig. 3c). However, only *Psu*ACR_353 generated a strong signal of a pH increase, indicating its significant Cl^- transport activity compared to the other ACRs.

Characterization of the anion transport activity of *Psu*ACR_353. To characterize the anion transport activity of *Psu*ACR_353, we measured the action spectrum and anion dependence of its transport activity using the pH electrode method. Fig. 4a shows that the Cl^- transport activities of *Psu*ACR_353 depend on the excitation light wavelength. Statistical comparisons of the initial slope amplitudes revealed that the activity at 530 nm was significantly larger than that at 590 nm (Fig. 4b). This result correlated well with a previous electrophysiological study [18]. We then measured the anion dependence of the transport activity of *Psu*ACR_353 using 530 nm light. Strong signals were observed not only for Cl^- but also for Br^-, I^-, NO_3^- and even SO_4^{2-} despite the low level of expression (Figs. 4c, 3b and 5b explained below). Especially for NO_3^-, the pH was increased by nearly 0.15 unit, which is ca. 3-times larger than even for the Cl^- transport of *Gt*ACR1 (Fig. 2f). In addition, statistical analysis clearly showed the strongest activity for NO_3^-, which was more than 2-times larger than that for the other anions (Fig. 4d). These results indicated that the anion selectivity of *Psu*ACR_353 was not restricted as was *Gt*ACR1 (Fig. 2g), however *Psu*ACR_353 preferably transported NO_3^-.

To quantitatively compare the anion transport activities of *Gt*ACR1 and *Psu*ACR_353, their expression levels were estimated by Western blotting (Figs. 5a and 5b). The results showed that the relative level of expression of *Psu*ACR_353 was ca. 0.46-times smaller than that of *Gt*ACR1. Fig. 5c and Supplementary Fig. S2 show statistical comparisons of the anion transport activities after correction to account for the expression levels of *Gt*ACR1 and *Psu*ACR_353. These results clearly showed that the transport activities of *Psu*ACR_353 for Cl^- and NO_3^- were ca. 2- and 5-times larger than that for *Gt*ACR1, respectively, and therefore the preference for NO_3^- of *Psu*ACR_353 was far greater than *Gt*ACR1 and other anion species.

Anion transport activities of *Gt*ACR1-C102T and *Psu*ACR_353-T108C mutants. Finally, the anion transport activities of mutant ACRs were investigated using the pH electrode method. As described in the previous section, one difference in the amino acid

sequence between *Gt*ACR1 and *Psu*ACR_353 is the amino acid conserved in the 3rd transmembrane helix, i.e. *Gt*ACR1 has Cys102 whereas *Psu*ACR_353 has Thr108 at that position (Table 1, Figs. 3a, 6a, and Supplementary Fig. S1). We investigated the effects of that difference on anion transport activity, anion selectivity and preference of *Gt*ACR1-C102T and *Psu*ACR_353-T108C mutants using the pH electrode method.

For the *Gt*ACR1-C102T mutant (Figs. 6b and 6c), the intensities of the pH change and initial slope increased compared to wild-type *Gt*ACR1 (Figs. 2f and 2g). However, the anion dependence was almost the same as the wild-type (Figs. 6c and 2g). The expression level of the *Gt*ACR1-C102T mutant was also not significantly different from the wild-type (Figs. 5a and 5b). Taking this into account, a statistical comparison showed that the transport activities of anions other than F^- were almost the same as those of the wild-type (Fig. 5c and Supplementary Fig. S2). On the other hand, when compared with the transport activities of wild-type *Psu*ACR_353, the transport activities of the *Gt*ACR1-C102T mutant were significantly smaller and the preference for NO_3^- was only slightly enhanced (Fig. 5c and Supplementary Fig. S2). Therefore, the Cys-to-Thr mutation at position 102 in *Gt*ACR1 resulted in almost no effect either on the anion transport activity or the selectivity or preference.

However, for the *Psu*ACR_353-T108C mutant (Figs. 6d and 6e), decreases in transport activities were observed for all anions by compared with wild-type *Psu*ACR_353 (Figs. 4c and 4d). In addition, the intensities of pH changes and initial slopes resulted in decreases to almost the same level (Figs. 6d and 6e), indicating that the anion dependence was completely lost due to that mutation. Taking into account the expression level of the *Psu*ACR_353-T108C mutant, which was about 7-times larger than wild-type *Gt*ACR1 (Figs. 5a and 5b), we concluded that the Thr-to-Cys mutation at position 108 in *Psu*ACR_353 caused a significant loss of function (Fig. 5c and Supplementary Fig. S2). These results indicate that the effects of the corresponding amino acids at positions 102 in *Gt*ACR1 and 108 in *Psu*ACR_353 on anion transport activity were completely different from each other, which would reflect the phylogenetic difference (Fig. 3a).

Discussion

In this study, we used the pH electrode method to measure the anion transport activity of ACRs expressed as recombinant proteins in yeast cells. That method has already been established and used for ion pump-type microbial rhodopsins expressed in *E. coli* cells. Therefore, this is the first study that measured the activity of ion channel-type rhodopsins expressed in yeast cells. The advantages of this method include the simple instrumental setup and the use of a glass electrode pH meter, and the ease of measurement even for non-experts in electrophysiology. Indeed, electrophysiological techniques are powerful and are required for quantitative and precise measurements of ion channel functions. However, as we demonstrate here, the action spectrum and the substrate dependence of anion transport activity can be easily measured using the pH electrode method. We assume that this method will also be useful as a screening technique to explore and engineer ACRs with unique absorptions, anion selectivities, and so on.

We newly characterize the strong anion transport activity and NO_3^- preference of *Psu*ACR_353 in this study. Govorunova et al. already performed electrophysiological measurements for various ACRs including *Psu*ACR_353 [18]. However, no results were reported for such preferences probably because they did not perform the electrophysiological measurements using various anions other than Cl^-. One reason for that we suppose is that the light-induced current of *Psu*ACR_353 caused by Cl^- transport was significantly smaller than not only the other ACRs tested but also for *Gt*ACR1 [4,18]. That may be due to the much lower expression levels of *Psu*ACR_353 in their mammalian cell expression system because its expression level was also significantly small even in our yeast expression system (Figs. 5a and 5b). We noticed that the magnitude relationship of the Cl^- transport activities of *Psu*ACR_353 and *Gt*ACR1 reported by Govorunova et al. [4,18] were completely different from our results obtained using the pH electrode method (Fig. 5c). This may also reflect differences in the expression levels of *Gt*ACR1 and *Psu*ACR_353 in each protein expression system.

On the other hand, the anion-dependent transport activity determined by each method can be considered equivalent. In the first report of *Gt*ACR1, its anion dependence was revealed by an electrophysiological method [4]. The result was that *Gt*ACR1 transported Cl^-, Br^-, I^- and NO_3^- almost equally but transported F^- more weakly. In this study, we were successfully reproduced such a dependence using the pH electrode method (Fig. 2g). The anion selectivity of *Gt*ACR1 is not restricted, which is similar to

the anion pump rhodopsins but different from the potassium channel. It is speculated that a structure or a mechanism working as an anion selective filter is not necessarily sophisticated in *Gt*ACR1. Conversely, such an unrestricted anion selectivity may be connected to its biological roles in the algae *G. theta*, which awaits clarification in further studies. In contrast, *Psu*ACR_353 was revealed to transport NO_3^- preferably to the other anions tested in this study (Figs. 4c, 4d, 5c and Supplementary Fig. S2). In the sense that *Psu*ACR_353 transported Cl^-, Br^- and I^- almost equally, which was the same as *Gt*ACR1, and even SO_4^{2-}, the anion selectivity was not restricted. However, the preference for NO_3^- was far greater than the other anions. To our knowledge, such a preference has not been discovered in any microbial pump- or channel-type rhodopsins reported so far.

Nitrate (NO_3^-) is one of the most stable forms of nitrogen on earth and is used as a nitrogen source by most organisms including plants [31]. For NO_3^- transport, both pump- and channel-type transporters exist in nature. Among them, a slowly activating anion channel 1 named SLAC1 and its homologous proteins named SLAH2 and SLAH3 expressed in plants are known to transport NO_3^- preferably and take part in nitrate acquisition in roots, in nitrate translocation from roots to shoots, and in guard cell closure [31,34]. Therefore, *Psu*ACR_353 may play a role in NO_3^- transport and might possibly take part in nitrate sensing and signaling, and furthermore, in the nitrogen assimilation in *P. sulcata* in nature. Indeed, it is known that *P. sulcata* senses the concentration of nitrate outside the cell and accumulates nitrogen as a form of protein-pigment, phycoerythrin, which contributes to the light-harvesting function for photosynthesis [35,36]. It should be noted that we tried to purify *Psu*ACR_353 to more deeply understand the mechanism and role of NO_3^- transport using spectroscopic techniques, but those efforts failed because the protein was unstable in the presence of a detergent.

We wonder why *Psu*ACR_353 is able to preferably transport NO_3^-. One possible explanation is that the ionic radii or hydrated radii of anions contribute to the preference [37]. However, no sequential correlation is seen because the ionic and hydrated radii of NO_3^- are 0.177 nm and 0.316 nm (Table 2), respectively, which is almost the same as those of Cl^- (0.180 nm and 0.319 nm, respectively). The crystallographic structure of *Gt*ACR1 in the dark state revealed that there is a continuous tunnel spanning through the protein, which is constructed by the 1^{st} – 3^{rd}, and 7^{th} transmembrane helices (Supplementary Fig. S1), and the radius of that tunnel is the same or smaller than the ionic radius of Cl^- (0.1 - 0.2 nm) [38,39]. More recently, it was revealed that the tunnel radius

is variable according to the anion species to be transported by *Gt*ACR1 [40]. Of course, a transient change of the tunnel radius accompanied by a structural change of the protein should also be considered because the structures of *Gt*ACR1 represent the state before light activation [38-40], and the unrestricted anion selectivity of *Gt*ACR1 can be explained by the size of the tunnel radius and the ionic radius of anions. Another possible explanation is that when *Psu*ACR_353 transports NO_3^- upon light activation, some spaces or sites are transiently formed, where NO_3^- is preferably trapped or passes through, during the photocycle. Among the anions we tested in this study, only NO_3^- is not spherically symmetrical. Thus, NO_3^- has two hydrated radii, one for the axial radius and another for the equatorial radius (Table 2) [37]. Therefore, it is speculated that a possible mechanism for the NO_3^- preference is that *Psu*ACR_353 transiently recognizes the asymmetrical structure of NO_3^- and therefore transports NO_3^- being hydrated.

We suppose that Thr108 in *Psu*ACR_353 is one of the residues contributing to the NO_3^- preference, which is based on comparisons of *Psu*ACR_353-T108C and *Gt*ACR1-C102T mutants (Figs. 5c, 6, and Supplementary Fig. S2). We investigated the effects of differences in amino acid residues at positions 102 and 108 in *Gt*ACR1 and in *Psu*ACR_353, respectively, on their anion transport activities, anion selectivity or preference for the first time in this study. Because the phylogenetic relationship between these ACRs is distant from each other (Fig. 3a), it is conceivable that the anion conducting paths and mechanisms in each ACR are different. The crystal structure of *Gt*ACR1 suggested that Cys102 is not involved in the anion conducting path [38-40]. On the other hand, in *Psu*ACR_353, Thr108 may be a part of a conducting path dedicated for NO_3^-.

Conclusion. In this study, we successfully demonstrated the usefulness of the pH electrode method to measure the anion transport activity of ACRs. This method allows us to measure the action spectra and the anion dependence of the transport activity simply and easily, with results comparable to previous results obtained using electrophysiological methods. In addition, we identified the strong anion transport activity and the preference for NO_3^- in *Psu*ACR_353 for the first time. Nitrate is one of the most stable forms of nitrogen and is used as a nitrogen source by most organisms including plants. Therefore, *Psu*ACR_353 may play a role in NO_3^- transport and might take part in NO_3^--related cellular functions in nature. Furthermore, we successfully

demonstrated that Thr108, which corresponds to Cys102 in *Gt*ACR1, contributes to the NO_3^- preference of *Psu*ACR_353. Such a preference has been discovered for the first time in microbial pump- or channel-type rhodopsins. This finding will be helpful to understand the anion transport mechanism of *Psu*ACR_353. We did not address the potential use of NO_3^--preferred *Psu*ACR_353 for optogenetics because NO_3^- is rare in mammalian cells. Possibly, *Psu*ACR_353 may be useful for optogenetics in plants.

Methods

DNA constructs of ACRs. Gene information about ACRs used in this study was obtained from GenBank and is summarized in Table 1. An 8 histidine tag was attached to the C-terminus of each ACR. The genes encoding ACRs with codon optimization for expression in *Pichia pastoris* were purchased from GENEWIZ (South Plainfield, NJ, U.S.A.). The procedures for constructing the pPICZ B vector (Thermo Fisher Scientific, Waltham, MA, U.S.A.) for *P. pastoris* were the same as our previous report [32]. The genes for *Gt*ACR1-C102T and *Psu*ACR_353-T108C mutants were prepared using PrimeSTAR Max DNA Polymerase (Takara Bio Inc., Shiga, Japan). The correctness of all nucleotide sequences was verified by dideoxy sequencing.

Protein expression. The methylotrophic yeast *Pichia pastoris* SMD1168H strain (Thermo Fischer Scientific) was used as the protein expression host. The procedures for transformation of yeast and for the protein expression were almost the same as our previous report [32]. Briefly, transformed *P. pastoris* SMD1168H cells were pre-cultured in BMGY medium containing 100 μg/mL Zeocin™ (Thermo Fisher Scientific) for 1 day at 30°C. The medium was exchanged to BMMY containing 100 μg/mL Zeocin™, 2% (v/v) methanol (Fuji Film Wako Chemical Industries, Co. Ltd., Japan) and 20 μM all-*trans*-retinal (Sigma-Aldrich, St. Louis, MO, U.S.A.), and protein expression was induced for 1 day at 30°C. The cells were collected by centrifugation (3,000 rpm, 5 min, 4 °C; himac CF16RN equipped with a T9A31 rotor; Hitachi Koki Co., Ltd., Tokyo, Japan).

Anion transport activity measurement and data analysis. To measure anion transport activity, *P. pastoris* SMD1168H cells expressing ACRs were washed with 300 mM salt solution (NaCl, NaF, NaBr, NaI, $NaNO_3$, Na_2SO_4, sodium aspartate; all from Fuji Film

Wako Chemical Industries) 4 times by centrifugation (3,000 rpm, 5 min, 4°C; himac CF16RN equipped with a T9A31 rotor). The cells were finally suspended in the same salt solution used for washing. As a negative control, *P. pastoris* SMD1168H cells without integration of any ACR gene were prepared. The optical density at 660 nm of each cell suspension was measured using a UV-1800 spectrophotometer (Shimadzu Corp., Kyoto, Japan) and adjusted to 1.9 on average. Anion transport activity was measured at temperatures below room temperature (16°C on average) by monitoring pH changes using a LAQUA F-72 pH meter equipped with a standard ToupH pH electrode (HORIBA, Ltd., Kyoto, Japan). To measure the dependence of transport activity on the wavelength of light, blue-green (peak wavelength is 505 nm), green (peak wavelength is 530 nm) and orange (peak wavelength is 590 nm) LED light was illuminated. The light intensity was adjusted to 10 mW/cm^2 on average, which was measured using a power meter (ORION, Ophir Optronics Solutions Ltd., Jerusalem, Israel). Anion transport activity was estimated by the initial slope of the first 10 sec after LED light illumination for the time-dependent pH changes. More than three independent measurements were averaged. For statistical analysis, one-way ANOVA followed by Dunnett's test and Tukey's test were performed using GraphPad Prism 9 software (GraphPad Software, San Diego, CA, U.S.A.).

SDS-PAGE and Western blotting. SDS-PAGE with 12% (v/v) polyacrylamide gels and Western blotting using an anti-His tag antibody conjugated with horseradish peroxidase (anti-His-tag mAb-HRP-DirecT, MBL Co., Ltd., Nagoya, Japan) were performed using standard protocols. *P. pastoris* cell samples were prepared as previously published [33]. Briefly, 1 mL of each cell suspension at an OD_{660} of ca. 1.9 was centrifuged to collect cell pellets. The wet weight of the cell pellets was 10 mg on average. The cell pellets were then resuspended in 1 mL 0.1 M NaOH and incubated for 5 min at room temperature. After centrifugation to remove the supernatant, the cell pellets were suspended in 250 μL SDS-PAGE sample buffer (60 mM Tris-HCl (pH 6.8), 2% (w/v) SDS, 5% (v/v) glycerol, 4% (v/v) β-mercaptoethanol and 0.0025% (w/v) bromophenol blue) and then boiled at 95°C for 5 min. Finally, after centrifugation again, 6 μL of each supernatant diluted by one-sixth was loaded on the gel. To estimate the total amount of each ACR expressed in *P. pastoris* cells, the band intensities were analyzed using ImageJ software (U.S. National Institutes of Health, Bethesda, MD, U.S.A.) and 5 independent measurements were

averaged. For statistical analysis, one-way ANOVA followed by Dunnett's test was performed using GraphPad Prism 9 software (GraphPad Software).

Acknowledgements

This research was supported by grants from the Japan Society for the Promotion of Science (Grant-in-Aid for Young Scientists, No. 18K1465808), from Hokkaido University Tenure Track System, and from Global Station for Soft Matter, a project of Global Institution for Collaborative Research and Education at Hokkaido University. The authors thank DASS Manuscript for English language editing.

Author contributions

T.T. designed the research. C.K., H.K., T.W. and T.T. performed experiments and analyzed data. M.D. and T.K. provided technical assistance. C.K. and T.T. wrote the paper. All authors discussed and confirmed the results of the paper.

Notes

The authors declare no competing financial interest.

References

1. Nagel, G. *et al.* Channelrhodopsin-1: a light-gated proton channel in green algae. *Science* **296,** 2395–2398 (2002).
2. Ernst, O. P. *et al.* Microbial and animal rhodopsins: structures, functions, and molecular mechanisms. *Chem. Rev.* **114,** 126–163 (2014).
3. Nagel, G. *et al.* Channelrhodopsin-2, a directly light-gated cation-selective membrane channel. *Proc Natl Acad Sci USA* **100,** 13940–13945 (2003).
4. Govorunova, E. G., Sineshchekov, O. A., Janz, R., Liu, X. & Spudich, J. L. Natural light-gated anion channels: A family of microbial rhodopsins for advanced optogenetics. *Science* **349,** 647–650 (2015).
5. Sineshchekov, O. A., Jung, K.-H. & Spudich, J. L. Two rhodopsins mediate

phototaxis to low- and high-intensity light in *Chlamydomonas reinhardtii*. *Proc Natl Acad Sci USA* **99,** 8689–8694 (2002).

6. Suzuki, T. *et al.* Archaeal-type rhodopsins in *Chlamydomonas*: model structure and intracellular localization. *Biochem Biophys Res Commun* **301,** 711–717 (2003).
7. Ernst, O. P. *et al.* Photoactivation of channelrhodopsin. *J. Biol. Chem.* **283,** 1637–1643 (2008).
8. Kianianmomeni, A., Stehfest, K., Nematollahi, G., Hegemann, P. & Hallmann, A. Channelrhodopsins of *Volvox carteri* are photochromic proteins that are specifically expressed in somatic cells under control of light, temperature, and the sex inducer. *Plant Physiol* **151,** 347–366 (2009).
9. Zhang, F. *et al.* Red-shifted optogenetic excitation: a tool for fast neural control derived from *Volvox carteri*. *Nat. Neurosci.* **11,** 631–633 (2008).
10. Govorunova, E. G., Sineshchekov, O. A., Li, H., Janz, R. & Spudich, J. L. Characterization of a Highly Efficient Blue-shifted Channelrhodopsin from the Marine Alga *Platymonas subcordiformis*. *J. Biol. Chem.* **288,** 29911–29922 (2013).
11. Govorunova, E. G., Spudich, E. N., Lane, C. E., Sineshchekov, O. A. & Spudich, J. L. New channelrhodopsin with a red-shifted spectrum and rapid kinetics from *Mesostigma viride*. *MBio* **2,** e00115–11 (2011).
12. Hou, S.-Y. *et al.* Diversity of Chlamydomonas channelrhodopsins. *Photochem Photobiol* **88,** 119–128 (2012).
13. Zhang, F. *et al.* The microbial opsin family of optogenetic tools. *Cell* **147,** 1446–1457 (2011).
14. Klapoetke, N. C. *et al.* Independent optical excitation of distinct neural populations. *Nat. Methods* **11,** 338–346 (2014).
15. Govorunova, E. G., Sineshchekov, O. A. & Spudich, J. L. *Proteomonas sulcata* ACR1: A Fast Anion Channelrhodopsin. *Photochem Photobiol* **92,** 257–263 (2016).
16. Wietek, J., Broser, M., Krause, B. S. & Hegemann, P. Identification of a Natural Green Light Absorbing Chloride Conducting Channelrhodopsin from *Proteomonas sulcata*. *J. Biol. Chem.* **291,** 4121–4127 (2016).
17. Govorunova, E. G. *et al.* The Expanding Family of Natural Anion Channelrhodopsins Reveals Large Variations in Kinetics, Conductance, and Spectral Sensitivity. *Sci. Rep.* **7,** 43358 (2017).

18. Govorunova, E. G. *et al.* Extending the Time Domain of Neuronal Silencing with Cryptophyte Anion Channelrhodopsins. *eNeuro* **5,** e0174–18 (2018).
19. Oppermann, J. *et al.* MerMAIDs: a family of metagenomically discovered marine anion-conducting and intensely desensitizing channelrhodopsins. *Nat Commun* **10,** 3315–13 (2019).
20. Wietek, J. *et al.* Anion-conducting channelrhodopsins with tuned spectra and modified kinetics engineered for optogenetic manipulation of behavior. *Sci. Rep.* **7,** 14957 (2017).
21. Rozenberg, A. *et al.* Lateral Gene Transfer of Anion-Conducting Channelrhodopsins between Green Algae and Giant Viruses. *Curr. Biol.* **30,** 4910–4920.e5 (2020).
22. Wietek, J. *et al.* Conversion of Channelrhodopsin into a Light-Gated Chloride Channel. *Science* **344,** 409–412 (2014).
23. Berndt, A., Lee, S. Y., Ramakrishnan, C. & Deisseroth, K. Structure-Guided Transformation of Channelrhodopsin into a Light-Activated Chloride Channel. *Science* **344,** 420–424 (2014).
24. Schneider, F., Grimm, C. & Hegemann, P. Biophysics of Channelrhodopsin. *Annu. Rev. Biophys.* **44,** 167–186 (2015).
25. Kato, H. E. *et al.* Structural mechanisms of selectivity and gating in anion channelrhodopsins. *Nature* **561,** 349–354 (2018).
26. Sineshchekov, O. A., Govorunova, E. G., Li, H. & Spudich, J. L. Gating mechanisms of a natural anion channelrhodopsin. *Proc Natl Acad Sci USA* **112,** 14236–14241 (2015).
27. Sineshchekov, O. A., Li, H., Govorunova, E. G. & Spudich, J. L. Photochemical reaction cycle transitions during anion channelrhodopsin gating. *Proc Natl Acad Sci USA* **113,** E1993–E2000 (2016).
28. Doi, S., Tsukamoto, T., Yoshizawa, S. & Sudo, Y. An inhibitory role of Arg-84 in anion channelrhodopsin-2 expressed in *Escherichia coli*. *Sci. Rep.* **7,** 41879 (2017).
29. Kojima, K. *et al.* Mutational analysis of the conserved carboxylates of anion channelrhodopsin-2 (ACR2) expressed in *Escherichia coli* and their roles in anion transport. *Biophys Physicobiol* **15,** 179–188 (2018).
30. Kojima, K. *et al.* Green-Sensitive, Long-Lived, Step-Functional Anion Channelrhodopsin-2 Variant as a High-Potential Neural Silencing Tool. *J. Phys.*

Chem. Lett. **11,** 6214–6218 (2020).

31. Vidal, E. A. *et al.* Nitrate in 2020: Thirty Years from Transport to Signaling Networks. *Plant Cell* **32,** 2094–2119 (2020).
32. Tsukamoto, T. *et al.* Implications for the impairment of the rapid channel closing of Proteomonas sulcata anion channelrhodopsin 1 at high Cl- concentrations. *Sci. Rep.* **8,** 13445 (2018).
33. Kushnirov, V. V. Rapid and reliable protein extraction from yeast. *Yeast* **16,** 857–860 (2000).
34. Maierhofer, T. *et al.* A Single-Pore Residue Renders the Arabidopsis Root Anion Channel SLAH2 Highly Nitrate Selective. *Plant Cell* **26,** 2554–2567 (2014).
35. Brown, S. B. *et al.* New trends in photobiology biosynthesis of phycobilins. Formation of the chromophore of phytochrome, phycocyanin and phycoerythrin. *J. Photochem. Photobiol. B* **5,** 3–23 (1990).
36. Faulkner, S. T. *et al.* Single-Cell and Bulk Fluorescence Excitation Signatures of Seven Phytoplankton Species During Nitrogen Depletion and Resupply. *Appl. Spectrosc.* **73,** 304–312 (2019).
37. Marcus, Y. Ionic radii in aqueous solutions. *Chem. Rev.* **88,** 1475–1498 (1988).
38. Li, H. *et al.* Crystal structure of a natural light-gated anion channelrhodopsin. *Elife* **8,** 213 (2019).
39. Kim, Y. S. *et al.* Crystal structure of the natural anion-conducting channelrhodopsin *Gt*ACR1. *Nature* **561,** 343–348 (2018).
40. Li, H. *et al.* The Crystal Structure of Bromide-Bound *Gt*ACR1 Reveals a Pre-Activated State. *bioRxiv***,** doi: https://doi.org/10.1101/2020.12.31.424927.

Tables

Table 1. Gene and amino acid information of ACRs used in this study.

Protein name abbreviation	Organism	Accession	68th residue in *Gt*ACR1	102th residue in *Gt*ACR1	Number of amino acids
*Gt*ACR1	*Guillardia theta* CCMP2712	KP171708	Glu	Cys	295
*Psu*ACR1	*Proteomonas sulcata* CCMP704	KF992074	Glu	Cys	291
ZipACR		KX879679	Glu	Cys	314
*Psu*ACR_353		MG831189	Glu	Thr	303
*Gc*ACR_145	*Geminigera cryophila* CCMP2564	KX879675	Glu	Cys	326
*Gc*ACR_197		MG831184	Glu	Val	332
*Gc*ACR_201		MG831185	Glu	Thr	288
*Gc*ACR_439		KX879676	Glu	Cys	340
*Gc*ACR_457		KX879674	Glu	Cys	316

Data taken from [4,15-18].

Table 2. Summary of ionic and hydrated radii of anions tested in this study.

Anion	Ionic radius / nm	Hydrated radius / nm
F^-	0.124	0.263
Cl^-	0.180	0.319
Br^-	0.198	0.337
I^-	0.225	0.365
NO_3^- mean	0.177	0.316
NO_3^- axial	-	0.265
NO_3^- equatorial	-	0.345
SO_4^{2-}	0.242	0.382

Data taken from [37].

Figure Legends

Figure 1. Illustration of the concept of the pH electrode method for measuring anion transport activity of ACRs expressed in yeast *P. pastoris* cells. In this system, ACRs import anions according their electrochemical potential gradient because the anion concentration outside the cells was kept higher (300 mM) than inside (nearly 0 mM). Therefore, a pH increase will be detected due to the secondary influx of protons to compensate the membrane potential being more negative due to the influx of anions.

Figure 2. Anion transport activity of *Gt*ACR1 measured using the pH electrode method. **(a)** Comparisons of Cl^- transport activities in the absence (black line) or presence of 10 μM CCCP (red line); the negative control (grey line) was yeast cells without integration of the *Gt*ACR1 gene. 530 nm LED light (10 mW/cm^2) was illuminated for 2 min as shown on a white background. **(b)** The color of pigmented yeast cell suspension expressing *Gt*ACR1 changed from pink to yellow by adding 10 μM CCCP, probably due to denaturation. **(c)** Comparisons of Cl^- transport activities at various excitation light wavelengths (10 mW/cm^2). LED lights were illuminated for 2 min as shown on a white background. **(d)** Statistical comparisons of Cl^- transport activities at various excitation light wavelengths. Data are reported as means and S.E.M.; the numbers in parentheses indicate the number of independent experiments. One-way ANOVA followed by Tukey's test was performed (p-value; *** < 0.0006). **(e)** Visible absorption spectrum of purified *Gt*ACR1 suspended in 10 mM MOPS (pH 7) buffer containing 1 M NaCl and 0.05% *n*-Dodecyl-β-D-maltoside (DDM). **(f)** Comparisons of anion-dependent transport activities. 530 nm LED light (10 mW/cm^2) was illuminated for 2 min as shown on a white background. **(g)** Statistical comparisons of anion-dependent transport activities. Data are reported as means and S.E.M.; the numbers in parentheses indicate the number of independent experiments. One-way ANOVA followed by Dunnett's test was performed (p-values; **** < 0.0001, *** 0.0001, ** 0.0084). The negative control was yeast cells without integration of the *Gt*ACR1 gene resuspended in 300 mM NaCl.

Figure 3. ACRs tested using the pH electrode method. **(a)** Phylogenetic relationship of 45 ACRs analyzed by MEGA 7 software. According to amino acids conserved at position 102 in *Gt*ACR1, ACRs are classified into three types, Cys-type (blue), Thr-type (green)

and Val-type (orange). **(b)** Pictures of pigmented yeast cells due to the functional expression of each ACR in the presence of all-*trans*-retinal. The negative control was yeast cells without integration of any ACR gene. **(c)** Comparisons of Cl^- transport activities of ACRs. LED lights were illuminated for 2 or 3 min as shown on a white background.

Figure 4. Anion transport activity of *Psu*ACR_353 measured using the pH electrode method. **(a)** Comparisons of Cl^- transport activities at various excitation light wavelengths (10 mW/cm^2). LED lights were illuminated for 2 min as shown on a white background. **(b)** Statistical comparisons of Cl^- transport activities at various excitation light wavelengths. Data are reported as means and S.E.M.; the numbers in parenthesis indicate the numbers of independent experiments. One-way ANOVA followed by Tukey's test was performed (p-value; * 0.0471). **(c)** Comparisons of anion-dependent transport activities. 530 nm LED light (10 mW/cm^2) was illuminated for 2 min as shown on a white background. **(d)** Statistical comparisons of anion-dependent transport activities. Data are reported as means and S.E.M.; the numbers in parentheses indicate the number of independent experiments. One-way ANOVA followed by Dunnett's test was performed (p-values; **** < 0.0001, *** 0.0002, * 0.0461). The negative control was yeast cells without integration of the *Psu*ACR_353 gene resuspended in 300 mM NaCl.

Figure 5. Quantitative comparisons of the anion transport activities of *Gt*ACR1, *Psu*ACR_353 and their mutants. **(a)** Western blotting using anti-His-tag mAb after SDS-PAGE; each ACR has monomer and dimer bands as indicated by filled and open triangles, respectively. The sum of band intensities was used to estimate protein expression levels. **(b)** Statistical comparisons of relative expression levels. Data are reported as means and S.E.M.; the numbers in parentheses indicate the number of independent experiments. One-way ANOVA followed by Dunnett's test was performed (p-values; **** < 0.0001, * 0.0124). **(c)** Statistical comparisons of the transport activities of Cl^- (left) and NO_3^- (right). Data were corrected by the relative expression level and are reported as means and S.E.M.; the numbers in parentheses indicate the number of independent experiments. One-way ANOVA followed by Tukey's test was performed (p-values; **** < 0.0001, *** < 0.0007, ** < 0.0049, * < 0.0492).

Figure 6. Anion transport activities of *Gt*ACR1-C102T and the *Psu*ACR_353-T108C mutants. **(a)** Location of the Cys102 residue in the *Gt*ACR1 structure (PDB ID 6CSM) [39]. Cys102 and the all-*trans*-retinylidene chromophore are shown in stick representation by PyMOL. **(b, d)** Comparisons of anion-dependent transport activities of **(b)** *Gt*ACR1-C102T and **(d)** *Psu*ACR_353-T108C mutants. 530 nm LED light (10 mW/cm^2) was illuminated for 2 min as shown on a white background. **(c, e)** Statistical comparisons of anion-dependent transport activities of **(c)** *Gt*ACR1-C102T and **(e)** *Psu*ACR_353-T108C mutants. Data are reported as means and S.E.M.; the numbers in parentheses indicate the number of independent experiments. One-way ANOVA followed by Dunnett's test was performed (p-values; for *Gt*ACR1-C102T **** < 0.0001, * 0.0197; for *Psu*ACR_353-T108C **** < 0.0001, *** < 0.0007, * 0.0338). Negative controls are yeast cells without integration of any ACR gene resuspended in 300 mM NaCl.

Figures

Figure 1.

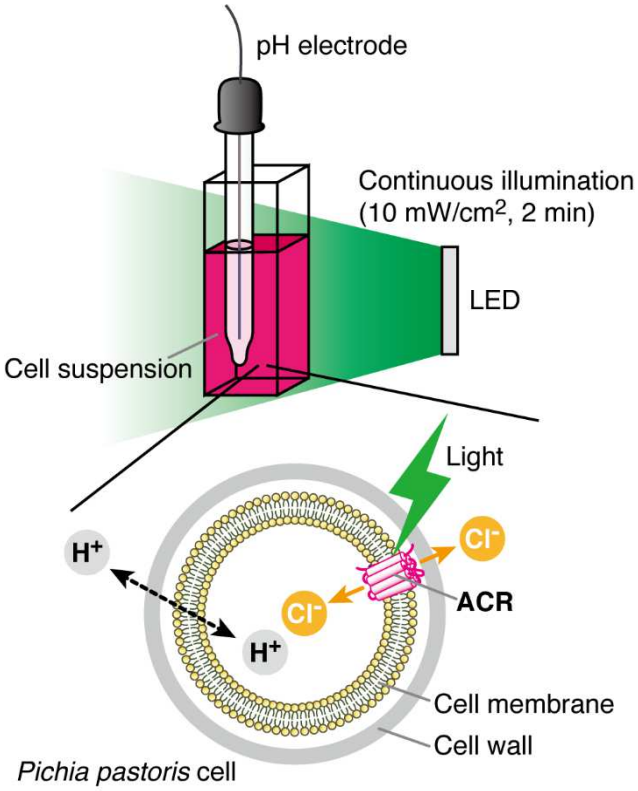

Figure 2.

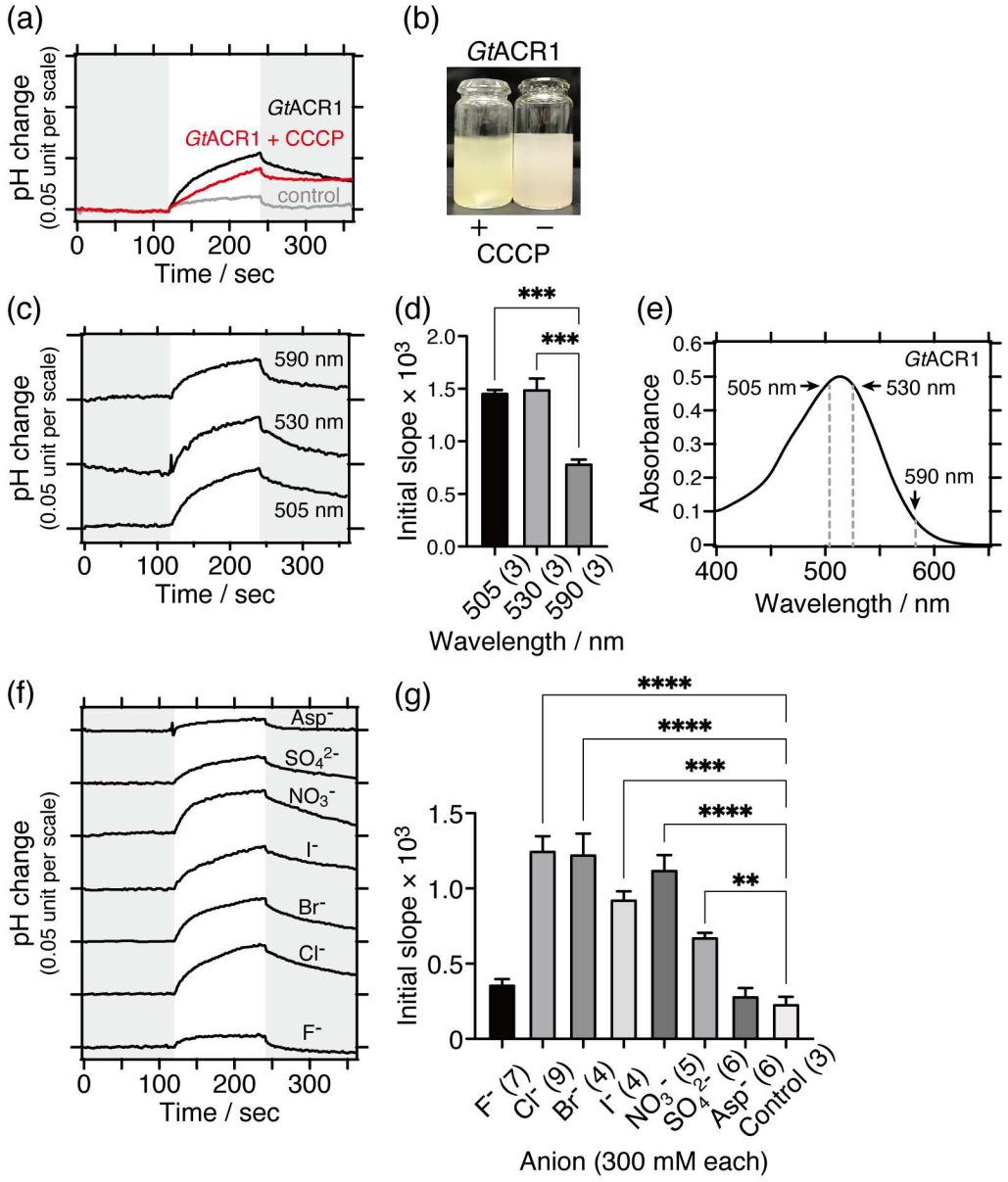
(a)
pH change
(0.05 unit per scale)
GtACR1
GtACR1 + CCCP
control
0
100
200
300
Time / sec
(b)
GtACR1
+
−
CCCP
(c)
pH change
(0.05 unit per scale)
590 nm
530 nm
505 nm
0
100
200
300
Time / sec
(d)
***
***
Initial slope x 10^3
2.0
1.5
1.0
0.5
0.0
505 (3)
530 (3)
590 (3)
Wavelength / nm
(e)
Absorbance
0.6
0.5
0.4
0.3
0.2
0.1
0
GtACR1
505 nm
530 nm
590 nm
400
500
600
Wavelength / nm
(f)
pH change
(0.05 unit per scale)
Asp-
SO4 2-
NO3-
I-
Br-
Cl-
F-
0
100
200
300
Time / sec
(g)
****
****
***
****
**
Initial slope x 10^3
1.5
1.0
0.5
0
F- (7)
Cl- (9)
Br- (4)
I- (4)
NO3- (5)
SO4 2- (6)
Asp- (6)
Control (3)
Anion (300 mM each)

Figure 3.

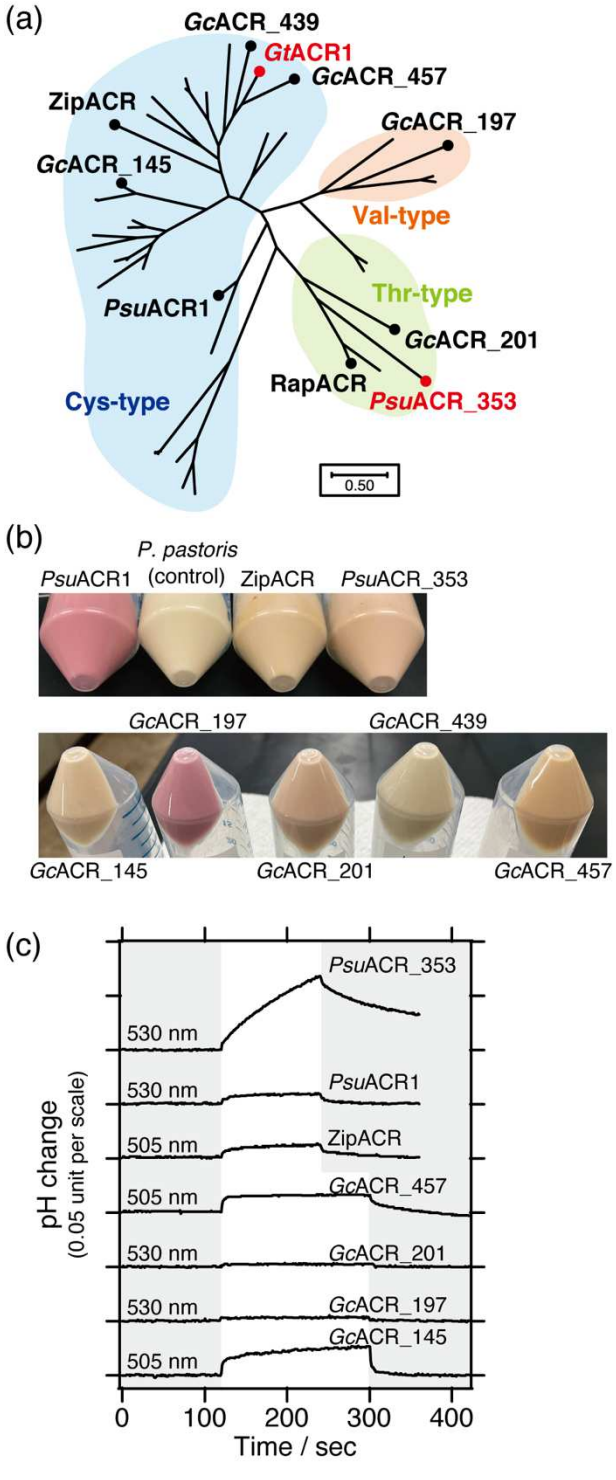
(a)
GcACR_439
GtACR1
GcACR_457
ZipACR
GcACR_197
GcACR_145
Val-type
Thr-type
PsuACR1
GcACR_201
RapACR
PsuACR_353
Cys-type
0.50
(b)
P. pastoris
PsuACR1 (control)
ZipACR
PsuACR_353
GcACR_197
GcACR_439
GcACR_145
GcACR_201
GcACR_457
(c)
PsuACR_353
530 nm
PsuACR1
530 nm
ZipACR
505 nm
GcACR_457
505 nm
GcACR_201
530 nm
GcACR_197
530 nm
GcACR_145
505 nm
pH change
(0.05 unit per scale)
0
100
200
300
400
Time / sec

Figure 4.

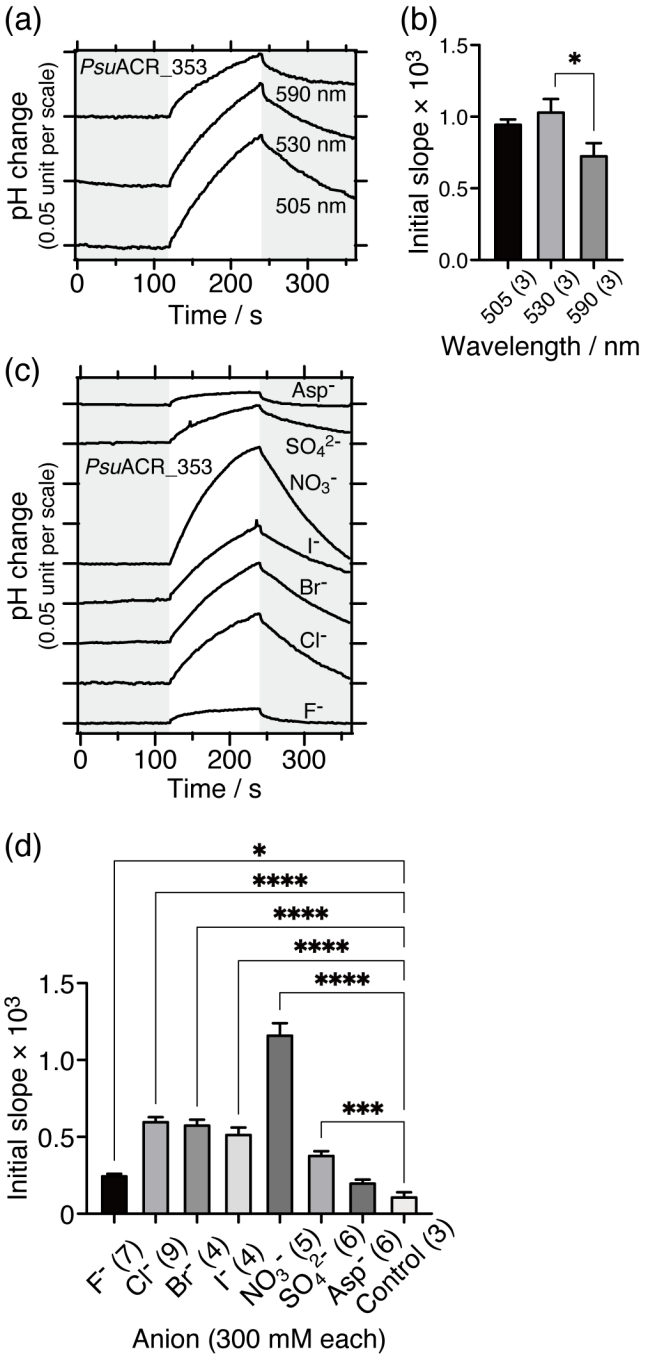
(a)
PsuACR_353
590 nm
530 nm
505 nm
pH change
(0.05 unit per scale)
0
100
200
300
Time / s
(b)
Initial slope × 10³
1.5
1.0
0.5
0.0
*
505 (3)
530 (3)
590 (3)
Wavelength / nm
(c)
Asp⁻
SO₄²⁻
PsuACR_353
NO₃⁻
I⁻
Br⁻
Cl⁻
F⁻
pH change
(0.05 unit per scale)
0
100
200
300
Time / s
(d)
*
****
****
****
****
***
Initial slope × 10³
1.5
1.0
0.5
0
F⁻ (7)
Cl⁻ (9)
Br⁻ (4)
I⁻ (4)
NO₃⁻ (5)
SO₄²⁻ (6)
Asp⁻ (6)
Control (3)
Anion (300 mM each)

Figure 5.

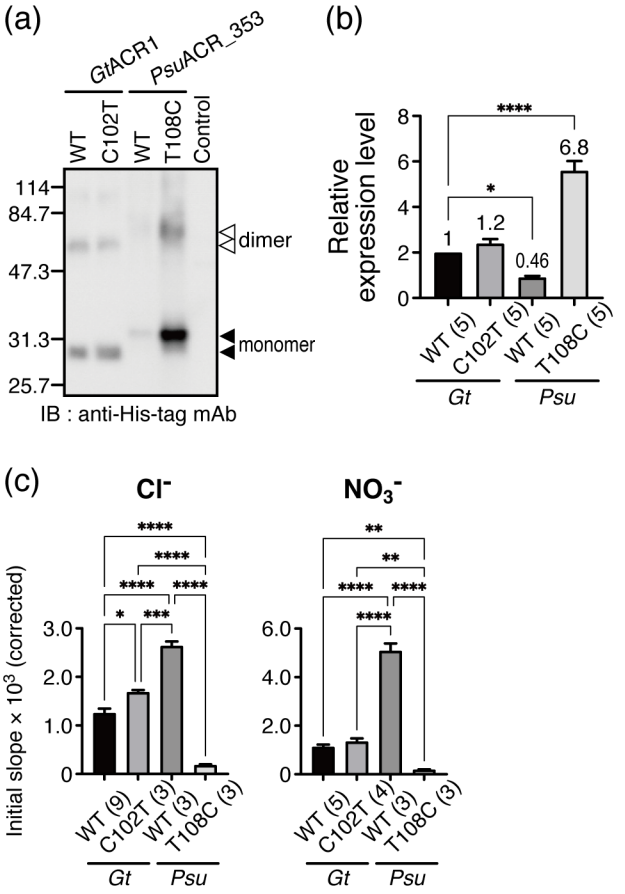
(a)
GtACR1
PsuACR_353
WT
C102T
WT
T108C
Control
114
84.7
47.3
31.3
25.7
dimer
monomer
IB : anti-His-tag mAb
(b)
Relative expression level
8
6
4
2
0
****
*
6.8
1.2
1
0.46
WT (5)
C102T (5)
WT (5)
T108C (5)
Gt
Psu
(c)
Cl-
NO3-
Initial slope × 10^3 (corrected)
****
****
****
****
*
***
3.0
2.0
1.0
0
WT (9)
C102T (3)
WT (3)
T108C (3)
Gt
Psu
**
**
****
****
****
6.0
4.0
2.0
0
WT (5)
C102T (4)
WT (3)
T108C (3)
Gt
Psu

Figure 6.

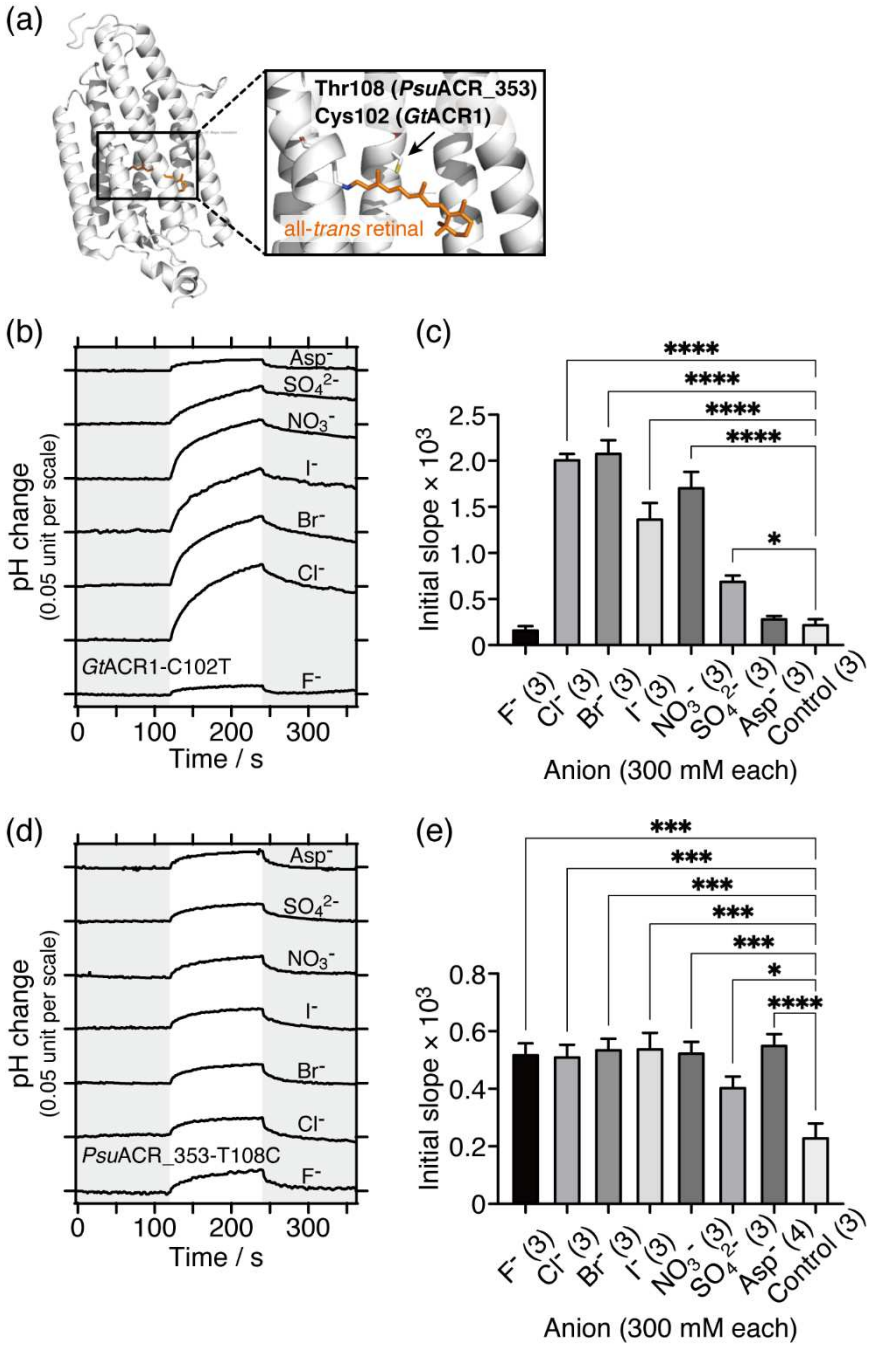
(a)
Thr108 (*Psu*ACR_353)
Cys102 (*Gt*ACR1)
all-*trans* retinal
(b)
pH change
(0.05 unit per scale)
Asp⁻
SO4 2-
NO3⁻
I⁻
Br⁻
Cl⁻
F⁻
*Gt*ACR1-C102T
0
100
200
300
Time / s
(c)
Initial slope × 10³
2.5
2.0
1.5
1.0
0.5
0
****
****
****
****
*
F⁻ (3)
Cl⁻ (3)
Br⁻ (3)
I⁻ (3)
NO3⁻ (3)
SO4 2- (3)
Asp⁻ (3)
Control (3)
Anion (300 mM each)
(d)
pH change
(0.05 unit per scale)
Asp⁻
SO4 2-
NO3⁻
I⁻
Br⁻
Cl⁻
F⁻
*Psu*ACR_353-T108C
0
100
200
300
Time / s
(e)
Initial slope × 10³
0.8
0.6
0.4
0.2
0
***
***
***
***
***
*
****
F⁻ (3)
Cl⁻ (3)
Br⁻ (3)
I⁻ (3)
NO3⁻ (3)
SO4 2- (3)
Asp⁻ (4)
Control (3)
Anion (300 mM each)

Figures

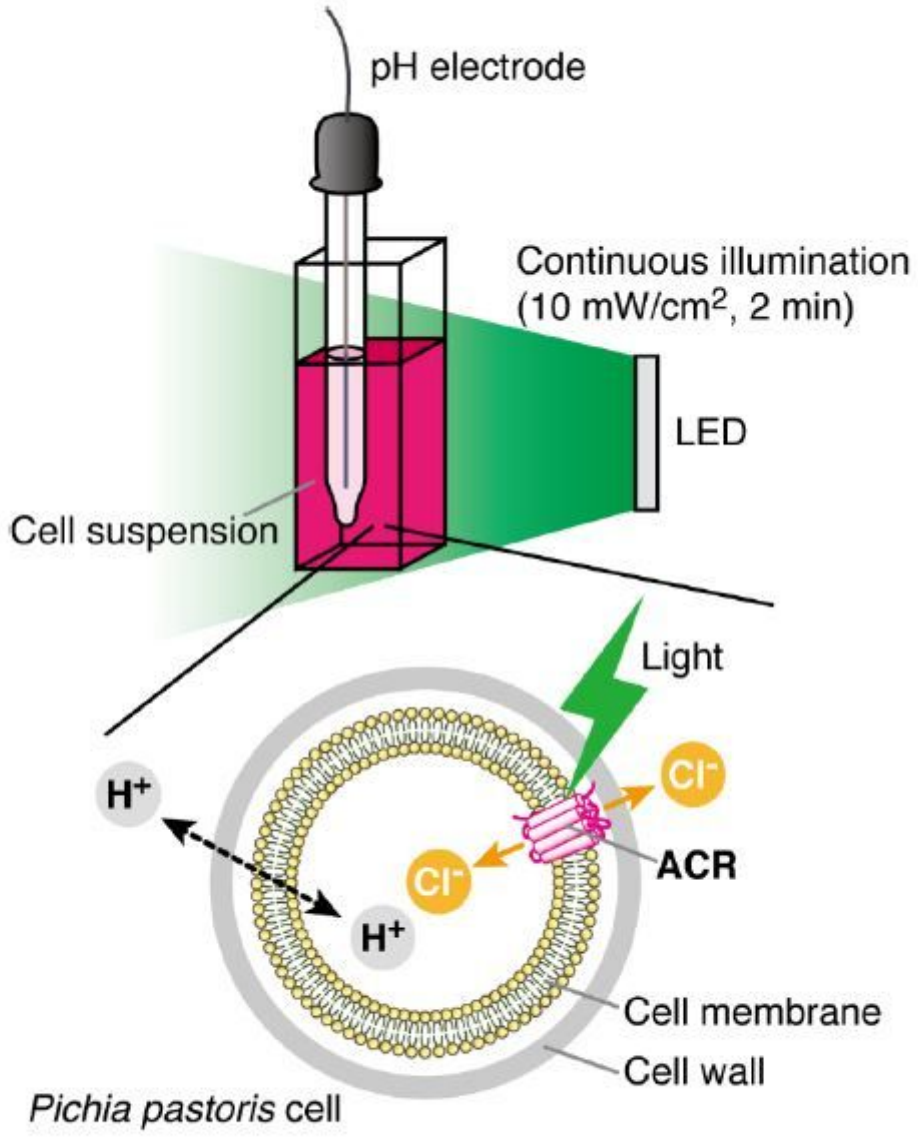

Figure 1

Illustration of the concept of the pH electrode method for measuring anion transport activity of ACRs expressed in yeast P. pastoris cells. In this system, ACRs import anions according their electrochemical potential gradient because the anion concentration outside the cells was kept higher (300 mM) than inside (nearly 0 mM). Therefore, a pH increase will be detected due to the secondary influx of protons to compensate the membrane potential being more negative due to the influx of anions.

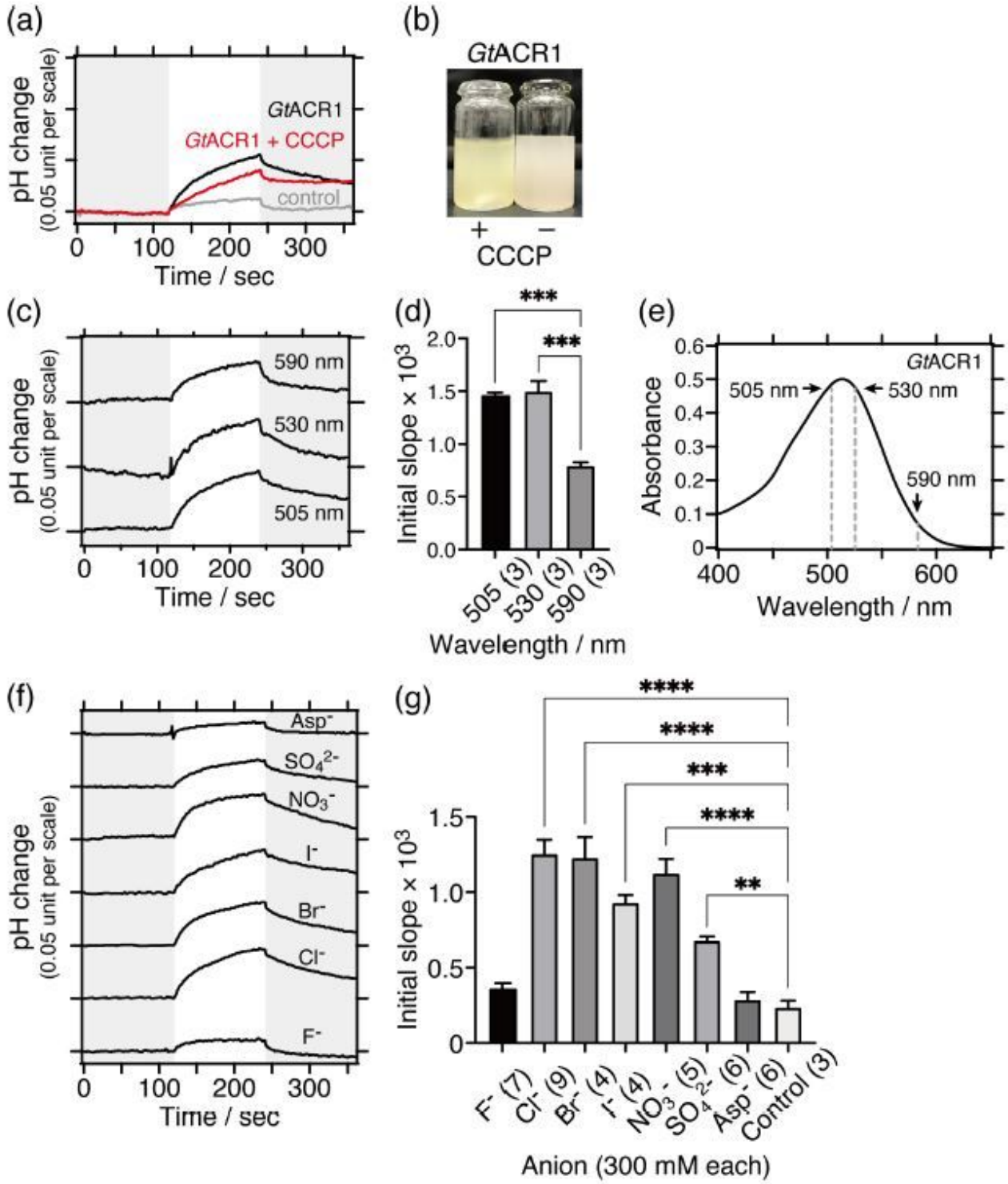

Figure 2

Anion transport activity of GtACR1 measured using the pH electrode method. (a) Comparisons of Cl- transport activities in the absence (black line) or presence of 10 μM CCCP (red line); the negative control (grey line) was yeast cells without integration of the GtACR1 gene. 530 nm LED light (10 mW/cm2) was illuminated for 2 min as shown on a white background. (b) The color of pigmented yeast cell suspension expressing GtACR1 changed from pink to yellow by adding 10 μM CCCP, probably due to denaturation. (c)

Comparisons of Cl- transport activities at various excitation light wavelengths (10 mW/cm2). LED lights were illuminated for 2 min as shown on a white background. (d) Statistical comparisons of Cl- transport activities at various excitation light wavelengths. Data are reported as means and S.E.M.; the numbers in parentheses indicate the number of independent experiments. One-way ANOVA followed by Tukey's test was performed (p-value; *** < 0.0006). (e) Visible absorption spectrum of purified GtACR1 suspended in 10 mM MOPS (pH 7) buffer containing 1 M NaCl and 0.05% n-Dodecyl-β-D-maltoside (DDM). (f) Comparisons of anion-dependent transport activities. 530 nm LED light (10 mW/cm2) was illuminated for 2 min as shown on a white background. (g) Statistical comparisons of anion-dependent transport activities. Data are reported as means and S.E.M.; the numbers in parentheses indicate the number of independent experiments. One-way ANOVA followed by Dunnett's test was performed (p-values; **** < 0.0001, *** 0.0001, ** 0.0084). The negative control was yeast cells without integration of the GtACR1 gene resuspended in 300 mM NaCl.

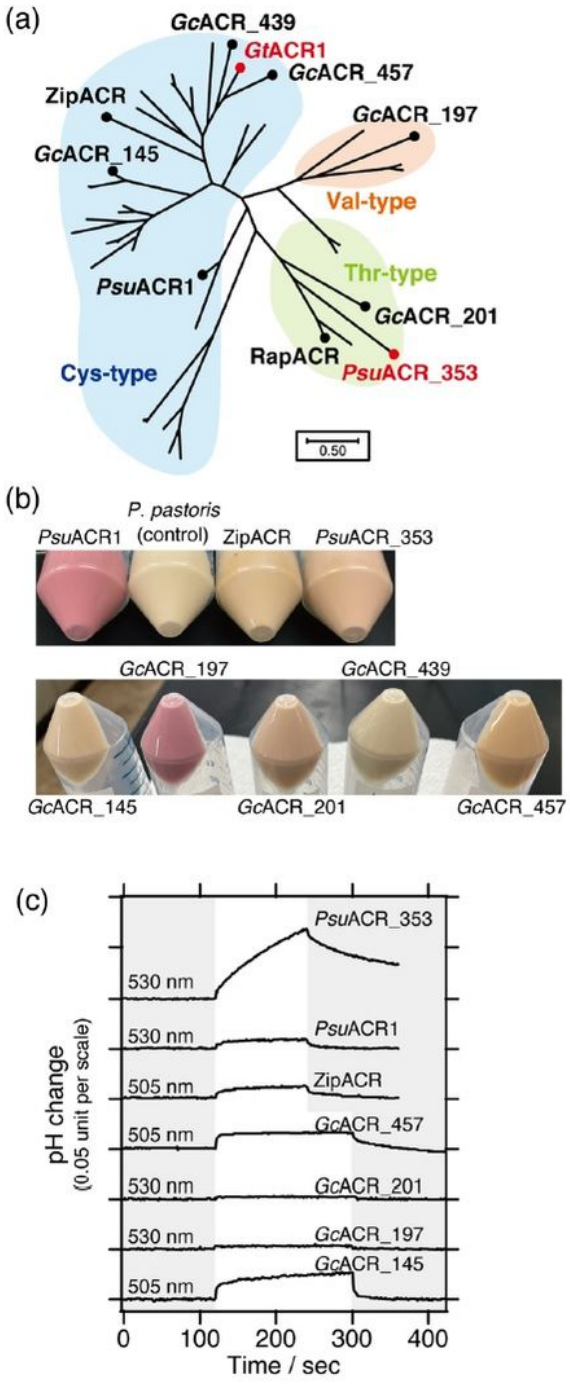

Figure 3

ACRs tested using the pH electrode method. (a) Phylogenetic relationship of 45 ACRs analyzed by MEGA 7 software. According to amino acids conserved at position 102 in GtACR1, ACRs are classified into three types, Cys-type (blue), Thr-type (green) and Val-type (orange). (b) Pictures of pigmented yeast cells due to the functional expression of each ACR in the presence of all-trans-retinal. The negative control was yeast

cells without integration of any ACR gene. (c) Comparisons of Cl- transport activities of ACRs. LED lights were illuminated for 2 or 3 min as shown on a white background.

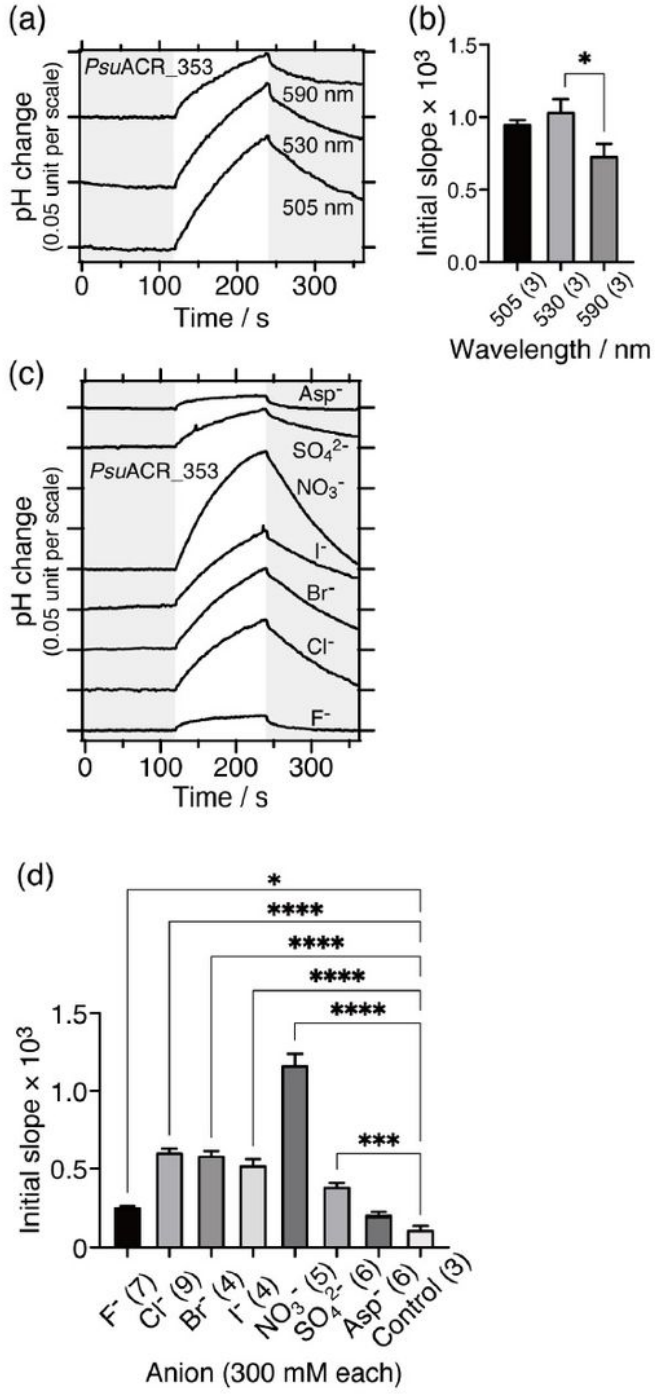

Figure 4

Anion transport activity of PsuACR_353 measured using the pH electrode method. (a) Comparisons of Cl- transport activities at various excitation light wavelengths (10 mW/cm2). LED lights were illuminated for 2 min as shown on a white background. (b) Statistical comparisons of Cl- transport activities at various

excitation light wavelengths. Data are reported as means and S.E.M.; the numbers in parenthesis indicate the numbers of independent experiments. One-way ANOVA followed by Tukey's test was performed (p-value; * 0.0471). (c) Comparisons of anion-dependent transport activities. 530 nm LED light (10 mW/cm2) was illuminated for 2 min as shown on a white background. (d) Statistical comparisons of anion-dependent transport activities. Data are reported as means and S.E.M.; the numbers in parentheses indicate the number of independent experiments. One-way ANOVA followed by Dunnett's test was performed (p-values; **** < 0.0001, *** 0.0002, * 0.0461). The negative control was yeast cells without integration of the PsuACR_353 gene resuspended in 300 mM NaCl.

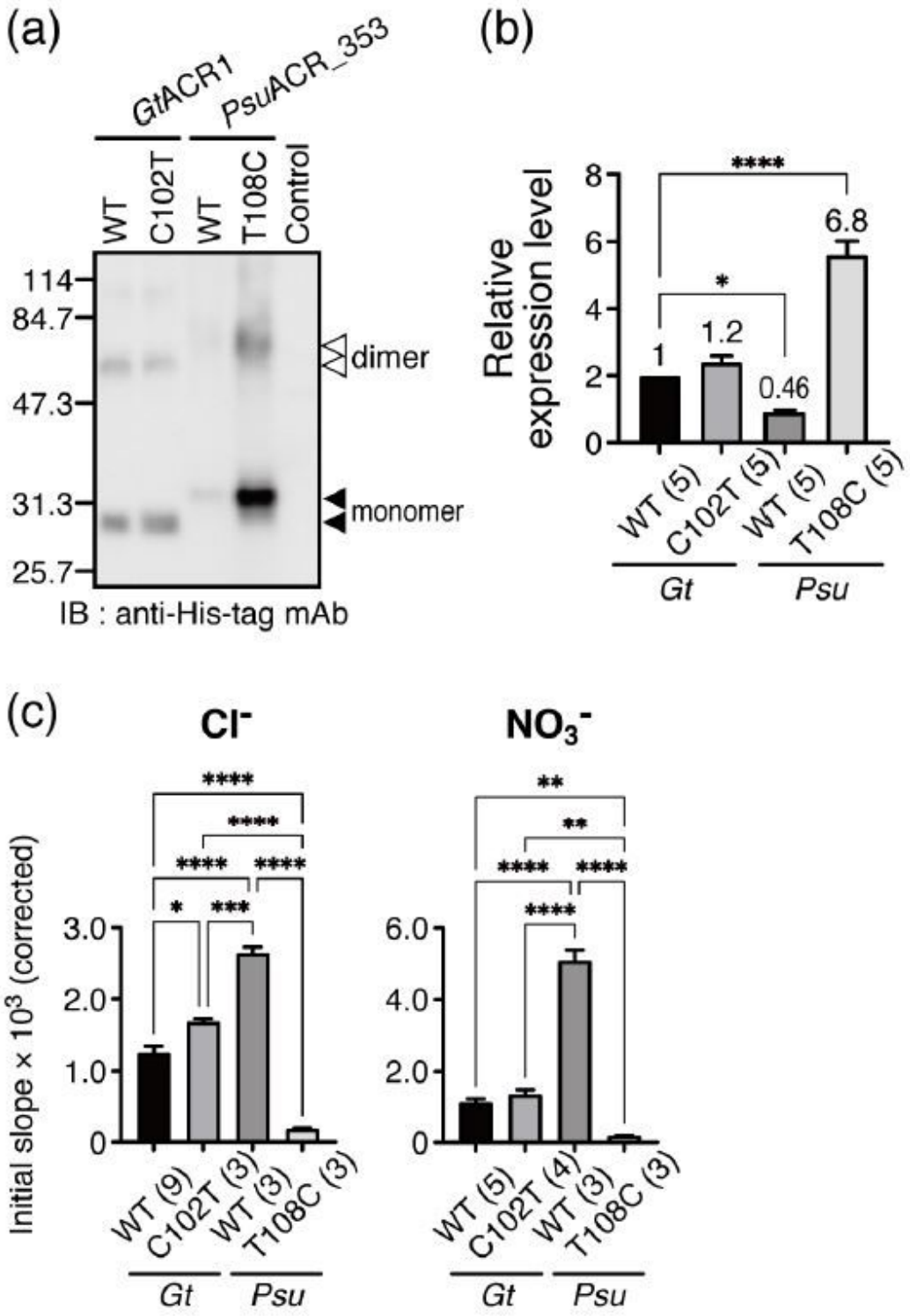

Figure 5

Quantitative comparisons of the anion transport activities of GtACR1, PsuACR_353 and their mutants. (a) Western blotting using anti-His-tag mAb after SDSPAGE; each ACR has monomer and dimer bands as indicated by filled and open triangles, respectively. The sum of band intensities was used to estimate protein expression levels. (b) Statistical comparisons of relative expression levels. Data are reported as means and S.E.M.; the numbers in parentheses indicate the number of independent experiments. One-

way ANOVA followed by Dunnett's test was performed (p-values; **** < 0.0001, * 0.0124). (c) Statistical comparisons of the transport activities of Cl- (left) and NO3- (right). Data were corrected by the relative expression level and are reported as means and S.E.M.; the numbers in parentheses indicate the number of independent experiments. One-way ANOVA followed by Tukey's test was performed (p-values; **** < 0.0001, *** < 0.0007, ** < 0.0049, * < 0.0492).

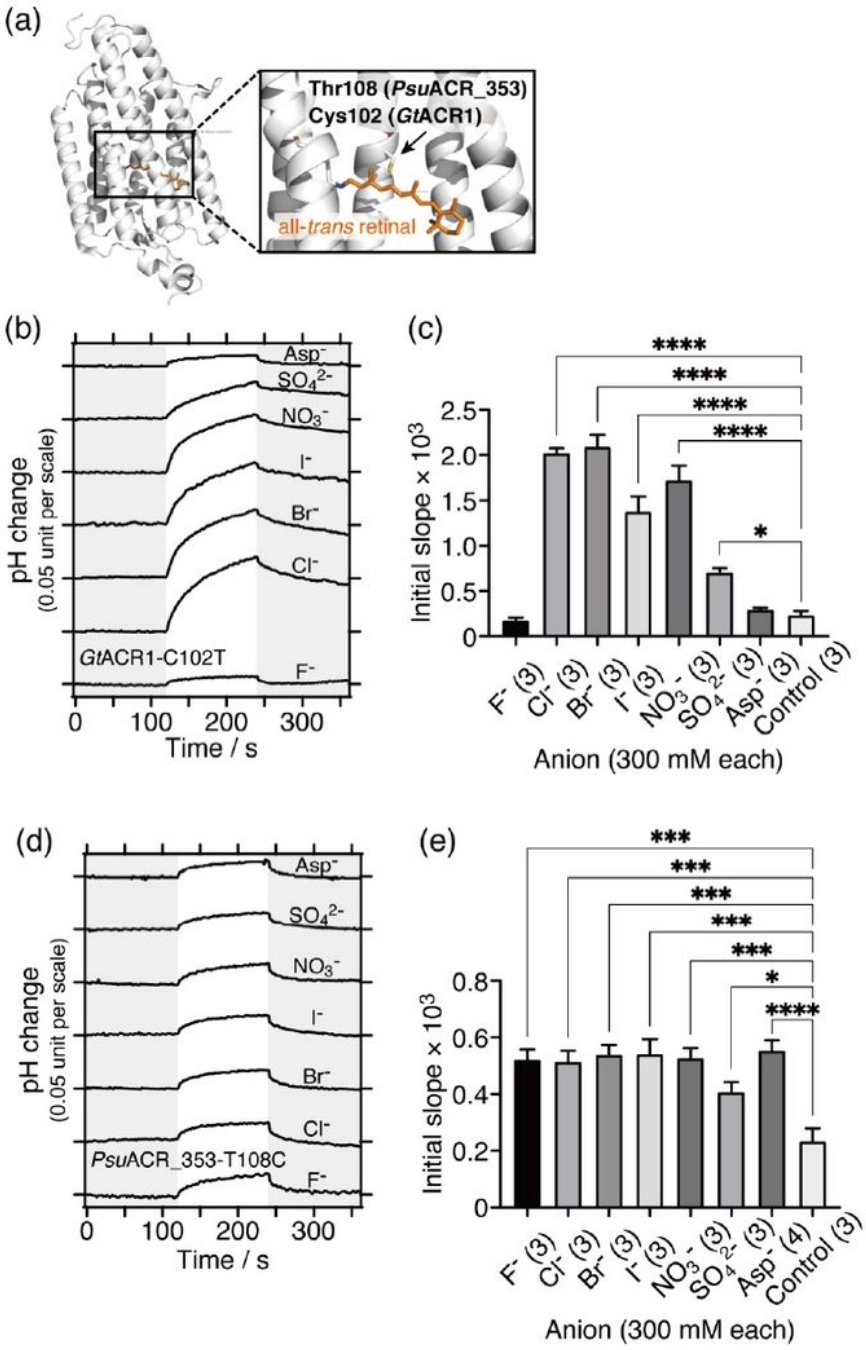

Figure 6

Anion transport activities of GtACR1-C102T and the PsuACR_353-T108C mutants. (a) Location of the Cys102 residue in the GtACR1 structure (PDB ID 6CSM) 39. Cys102 and the all-trans-retinylidene chromophore are shown in stick representation by PyMOL. (b, d) Comparisons of anion-dependent transport activities of (b) GtACR1-C102T and (d) PsuACR_353-T108C mutants. 530 nm LED light (10 mW/cm2) was illuminated for 2 min as shown on a white background. (c, e) Statistical comparisons of anion-dependent transport activities of (c) GtACR1-C102T and (e) PsuACR_353-T108C mutants. Data are reported as means and S.E.M.; the numbers in parentheses indicate the number of independent experiments. One-way ANOVA followed by Dunnett's test was performed (p-values; for GtACR1-C102T **** < 0.0001, * 0.0197; for PsuACR_353-T108C **** < 0.0001, *** < 0.0007, * 0.0338). Negative controls are yeast cells without integration of any ACR gene resuspended in 300 mM NaCl.

Supplementary Files

This is a list of supplementary files associated with this preprint. Click to download.

- 210123SupplementaryInformation.pdf